Atmos. Chem. Phys. Discuss., 13, 19837–19852, 2013
www.atmos-chem-phys-discuss.net/13/19837/2013/
doi:10.5194/acpd-13-19837-2013

Atmospheric Chemistry and Physics Discussions

Increased absorption by giant aerosol particles over the Gangetic–Himalayan region

V. S. Manoharan, R. Kotamarthi, Y. Feng, and M. P. Cadeddu

Environmental Science Division, Argonne National Laboratory, Argonne, Illinois, USA

Received: 25 June 2013 – Accepted: 13 July 2013 – Published: 26 July 2013

Correspondence to: V. S. Manoharan (vmanoharan@anl.gov)

Published by Copernicus Publications on behalf of the European Geosciences Union.

Abstract

Each atmospheric aerosol type has distinctive light-absorption characteristics related to its physical/chemical properties. Climate models treat black carbon as the light-absorbing component of all carbonaceous atmospheric aerosols. Most absorbing aerosols are assumed to be < 1 µm in diameter (sub-micron). Here we present results from a recent field study in India, primarily during the post-monsoon season (October–November), suggesting the presence of absorbing aerosols sized 1–10 µm. Absorption due to super-micron-sized particles was nearly 30 % greater than that due to smaller particles. Periods of increased absorption by larger particles ranged from a week to a month. Radiative forcing calculations under clear-sky conditions show that super-micron particles account for nearly 44 % of the total aerosol-forcing. The origin of the large aerosols is unknown, but meteorological conditions indicate that they are of local origin. Such economic and habitation conditions exist throughout much of the developing world. Hence, large absorbing particles could be an important component of the regional-scale atmospheric-energy balance.

1 Introduction

The Ganges Valley region is one of the most rapidly developing and densely populated regions in the northern part of the Indian subcontinent. In recent decades, this region has experienced increasing emissions of aerosols arising from fossil fuel, biofuel and biomass burning, besides mineral dust from the Thar Desert (Chinnam et al., 2006). Atmospheric aerosols scatter and absorb solar radiation and have the ability to modify regional and, to some extent, global climate forcing (e.g., Lau and Kim, 2006; Ramanathan et al., 2005; Gautam et al., 2007). Several observational and modeling studies have addressed the properties of aerosols in this region and their impact on monsoon rainfall in southern Asia (Bahadur et al., 2012; Costabile et al., 2012; Russell et al., 2010; Bergstrom et al., 2002; Dubovik et al., 2002). To investigate the regional im-

ACPD
13, 19837–19852, 2013

pact of aerosols on radiative transfer and cloud processes, the Ganges Valley Aerosol Experiment (GVAX) was conducted from June 2011 to March 2012 at Manora Peak, Nainital, India (29°21′ N, 79°27′ E).

The GVAX project was a joint study conducted by the US Department of Energy, Atmospheric Radiation Measurement Program, and the Indian Institute of Science, Bangalore, India. During this study, instruments for ground-level measurements of various atmospheric dynamics, cloud properties and radiative transfer were deployed at the Aryabhatta Research Institute of Observational Sciences, Nainital, approximately 280 km northeast of New Delhi. The site is situated at an altitude of roughly 1980 m a.m.s.l. (above the mean sea level) in the foothills of the Himalayan mountain range, far from major pollution sources such as industries and large metropolitan areas. Regions to the south and southwest of the observation site have low elevation (< 200 m a.m.s.l.) and merge with the vast Ganges basin. Additional details of the project are in Kotamarthi (2011).

2 Aerosol absorption and scattering measurements

In situ aerosol properties were measured continuously at the research institute at Nainital. A three-wavelength particle soot absorption photometer (470, 528 and 660 nm) was used to measure the particle absorption coefficient (σ_{abs}), and a three-wavelength nephelometer (450, 550 and 700 nm) measured the total particle scattering coefficient (σ_{scat}) and hemispheric back-scattering coefficient. The photometer and nephelometer switched between aerosol particles of diameter < 10 µm and < 1 µm ($D_{10\,\mu m}$ and $D_{1\,\mu m}$, respectively) every 30 min. Measuring in two aerosol size ranges allowed optical measurement of both fine- and coarse-mode aerosols, which often have different sources. The details of instrument operation, associated uncertainty limits and corrections applied can be found at http://www.arm.gov/sites/amf/pgh/.

ACPD
13, 19837–19852, 2013

3 Observations and analysis

3.1 Absorption properties of aerosols

The daily variations of aerosol absorption coefficients measured by the photometer at three wavelength bands (470, 528 and 660 nm) for $D_{1\,\mu m}$ and $D_{10\,\mu m}$ aerosol particles during the entire observation period are shown in Fig. 1. Absorption shows dependence on wavelength – decreasing absorption with increasing wavelength (Bergstrom et al., 2007). During the Indian summer monsoon of July–September 2011 (days 22–83 in Fig. 1) a significant decrease in aerosol absorption and scattering was observed throughout the 24 h day, with an average absorption coefficient of approximately 7 $M m^{-1}$ at the three wavelengths in visible spectrum. This is due to the aerosols washout from the atmosphere by continuous rainfall. However, during the post-monsoon season, absorption increased. Averaged over the nine months of observations, the mean value of the aerosol absorption coefficient was roughly 18 $M m^{-1}$. Another distinctive feature indicates that for approximately 10 h between 16:00 and 02:00 UTC (21:30 to 07:30 LT); the absorption was low on most of the days after monsoon. The exception was during the last week of October and the first two weeks in November 2011 (days 140–160), when a fair amount of high-intensity absorption was observed throughout the day. The absorption was highest for the $D_{10\,\mu m}$ particles (see Supplement Fig. S1 and Supplement Note A). This period (days 140–160) coincides with the beginning of post-harvest biomass burning over northwestern India (Sahai et al., 2012).

3.2 Absorption coefficient spectral index

The time series of daily averaged absorption coefficient values at the 470 nm and 660 nm wavelength for $D_{1\,\mu m}$ and $D_{10\,\mu m}$ particles are shown in Fig. 2a. The measurements made at 660 nm for $D_{1\,\mu m}$ particles and at 470 nm for $D_{10\,\mu m}$ particles represent the lowest and highest levels of absorption, respectively. However, the difference be-

ACPD
13, 19837–19852, 2013

tween these two extreme levels of absorption increases and decreases at different times of the year. For a given size of the particle (1 or 10 µm), on the log-log scale, the coefficient of absorption decreases nearly linearly with increasing of wavelength and the slope of the best fit straight line provides the absorption spectral index. A clear view of absorption characteristics is obtained from the daily average spectral index estimates across the three wavelengths (Fig. 2b). The absorption spectral index (ASI) is a slope determined separately for $D_{1\,\mu m}$ and $D_{10\,\mu m}$ ($ASI_{1\,\mu m}$ and $ASI_{10\,\mu m}$, respectively) measurements by fitting the best straight line to the corresponding logarithmic daily averages of absorption coefficients at the three wavelengths. The wavelength dependence of the absorption coefficient is often defined as $\frac{\sigma_{abs\lambda 1}}{\sigma_{abs\lambda 2}} = \left(\frac{\lambda_1}{\lambda_2}\right)^{ASI}$, where $\sigma_{abs\lambda 1}$ and $\sigma_{abs\lambda 2}$ are the absorption coefficients at two wavelength bands λ_1 and λ_2, and ASI is the negative slope of absorption vs. wavelength in a log-log plot.

Figure 2b shows that the daily averages of $ASI_{1\,\mu m}$ and $ASI_{10\,\mu m}$ take similar shapes during the entire period of observation, though their magnitudes are not always the same. The periods when the magnitudes of $ASI_{1\,\mu m}$ and $ASI_{10\,\mu m}$ are very different are indicated with yellow shading. These differences in the magnitudes of $ASI_{1\,\mu m}$ and $ASI_{10\,\mu m}$ follow a pattern similar to the observed differences in absorption coefficient (Fig. 2a). Furthermore, all of the shaded regions in Fig. 2b arise when $ASI_{10\,\mu m} > ASI_{1\,\mu m}$, indicating a flattening of the $ASI_{10\,\mu m}$ spectrum. This, in turn, implies that the $ASI_{10\,\mu m}$ spectrum is becoming much less dependent on the wavelength. A flatter $ASI_{10\,\mu m}$ spectrum for $D_{10\,\mu m}$ particles can result because of (1) a reduction in absorption at 470 nm with respect to 660 nm and/or (2) enhanced absorption at 660 nm with respect to 470 nm and/or (3) a relatively high absorption at all wavelengths, causing less difference between the values at 470 nm and 660 nm. Overall, this distinct feature indicates the presence of larger particles. Thus, when $ASI_{10\,\mu m} > ASI_{1\,\mu m}$, super-micron particles are in abundance. Conversely, when $ASI_{10\,\mu m} \leq ASI_{1\,\mu m}$, submicron particles are the dominant component. These results suggest that significant amounts of super-micron-sized particles were loaded continuously into the ambient aerosol, causing a steady increase in absorption. Eck et al. (2010) also suggested

ACPD
13, 19837–19852, 2013

the possibility of anomalously strong absorption in coarse mode aerosols in observations made at two AERONET sites (Beijing and Xianghe) located in the eastern China. These two sites are in or near downwind of the heavy metropolitan pollution, whereas our area of study, Nainital is away from major cities and at high elevation. The aerosols discussed here are likely from local sources as discussed later.

The average values of $ASI_{1\,\mu m}$ and $ASI_{10\,\mu m}$ are, respectively, −0.85 and −0.80. The average values of ASI before and after monsoon (before and after day 100) were −0.70 and −0.95, respectively, for both $D_{1\,\mu m}$ and $D_{10\,\mu m}$, indicating steepening of the absorption spectrum after the monsoon period. In Fig. 2b, the gap between $ASI_{1\,\mu m}$ and $ASI_{10\,\mu m}$ stays nearly constant between days 140 and 160, corresponding to the three-week period in October–November 2011 when increased absorption was also observed throughout the day (see Supplement Fig. S1 and Supplement Note A).

The plot of $ASI_{1\,\mu m}$ vs. $ASI_{10\,\mu m}$ (Fig. 2c) illustrates an overall correlation of approximately 90 %, with most of the data points lying close to the one-to-one line. The lower absorption by $D_{10\,\mu m}$ vs. $D_{1\,\mu m}$ particles is associated mostly with regions in Fig. 2b having near-constant values over multi-day periods (shaded yellow areas corresponding to the presence of super-micron-sized aerosol particles in the atmosphere).

3.3 Scattering properties of aerosols

The daily variations of aerosol scattering coefficients observed by the nephelometer for the $D_{1\,\mu m}$ and $D_{10\,\mu m}$ particles in wavelength bands at 450, 550 and 700 nm over the entire observation period (see Supplement Fig. S2 and Supplement Note B) demonstrate that scattering intensity decreases with wavelength. Moreover, these diurnal variations in scattering coefficient resemble the absorption coefficient variations shown in Fig. 1. As mentioned earlier, due to washout of aerosols by continuous rainfall, low aerosol scattering was observed during monsoon (July–September). After monsoon, aerosol scattering increased, with a peak centered at 06:30 UTC (local noon) daily. Scattering reached a maximum during the first week of November (roughly day 150).

ACPD
13, 19837–19852, 2013

3.4 Scattering coefficient spectral index

Time series of daily averaged scattering coefficient values in the 450 nm and 700 nm wavelength bands for $D_{1\,\mu m}$ and $D_{10\,\mu m}$ particles are shown in Fig. 3a. The measurements at 700 nm for $D_{1\,\mu m}$ particles represent the lower side of the scattering, while the highest values are observed at 450 nm for $D_{10\,\mu m}$ particles. As for absorption, the wavelength dependence of the scattering coefficient was used to compute scattering coefficient spectral index (SSI) for $D_{1\,\mu m}$ and $D_{10\,\mu m}$ particles ($SSI_{1\,\mu m}$ and $SSI_{10\,\mu m}$, respectively). During monsoon (before day 100) the scattering was low, as expected, averaging roughly 25 $M\,m^{-1}$ for both $D_{1\,\mu m}$ and $D_{10\,\mu m}$ particles. After the monsoon period (after approximately day 100), the scattering level and the SSI increased, peaking at about day 140. These results are consistent with those for absorption. However, as Fig. 3b shows, the daily average $SSI_{1\,\mu m}$ and $SSI_{10\,\mu m}$ values differ remarkably from the averages for the absorption spectra. Also, irrespective of season, the difference between $SSI_{10\,\mu m}$ and $SSI_{1\,\mu m}$ does not change significantly as indicated by the gap between $SSI_{10\,\mu m}$ and $SSI_{1\,\mu m}$. The averages of $SSI_{1\,\mu m}$ and $SSI_{10\,\mu m}$ are, respectively, −0.90 and −0.54. A nearly constant ratio of approximately 0.6 between these spectra indicates that the scattering is high for $D_{10\,\mu m}$ particles at all wavelength bands, leading to the flatness in the spectrum.

The plot of $SSI_{1\,\mu m}$ vs. $SSI_{10\,\mu m}$ yields a correlation coefficient of about 83 % (Fig. 3c). As the ratio of spectral indices reveals, the correlation shows an offset of roughly 0.6 with respect to the one-to-one correlation line. Further, during most of the observation period, $SSI_{10\,\mu m}$ spectra are flatter than $SSI_{1\,\mu m}$ spectra. As indicated by the daily average scattering coefficient plot (Fig. 3a and b), these periods correspond to a higher level of scattering.

3.5 Emission source location analysis

Measurements of surface wind from GVAX (Supplement Fig. S3 and Supplement Note C) indicate that the wind direction at Nainital was commonly from northwest and

ACPD
13, 19837–19852, 2013

southeast. Figure 4 shows HYSPLIT five-day back-trajectory analyses ending at 500 m and 2500 m a.g.l. over Nainital during October 2011. Trajectories at the 500 m level illustrate that the air masses most commonly originated in the nearby valley. This observation indicates that the strongly absorbing $D_{10\,\mu m}$ particles observed during GVAX were likely from local sources. In contrast, for the back-trajectories ending at the 2500 m level over Nainital, air masses generally originated from far northwestern and south-central India and remained above the boundary layer (altitude > 2500 m a.m.s.l.). This latter type of air mass is likely to carry mixtures of biomass burning aerosols above the boundary layer from the post-harvest agricultural burning in the northwestern states of Punjab and Haryana.

3.6 Implications of super-micron-sized particles for direct radiative forcing

Here, we explore the significance of the present findings for aerosol direct radiative forcing. A single-column Monte Carlo radiative transfer model (Kim and Ramanathan, 2008) was used to estimate forcing due to the abundance and increased absorption of super-micron-sized particles during the three-week period in October–November 2011 when a large fraction of total aerosol absorption near the surface was observed to be contributed by super-micron-sized particles (i.e., about 20 % more at 525 nm and even more at smaller wavelengths – about 30 % more at 470 nm). The radiation model adopts a surface albedo of 0.18 from the European Centre for Medium-Range Weather Forecasts surface solar radiation reanalysis over Nainital.

The GVAX surface measurements of aerosol extinction and absorption coefficients and the derived spectral indices were used to calculate aerosol optical depth and single scattering albedo for $D_{1\,\mu m}$ and $D_{10\,\mu m}$ particles. We assumed that the aerosols over Nainital were concentrated in the surface layer, up to 500 m a.g.l. The calculated column-integrated aerosol optical depth for aerosol particles was similar to the values retrieved from multifilter rotating shadowband radiometer measurements (0.1 ± 0.05) at 550 nm.

ACPD
13, 19837–19852, 2013

The estimated clear-sky direct radiative forcing of aerosol particles for this period was $-5.2\,\mathrm{W\,m^{-2}}$ at the top of the atmosphere, with roughly 44 % of the total aerosol forcing attributed to super-micron-sized particles. Because of the strong absorption in the shortwave range, the atmospheric absorption and the heating effect due to super-micron aerosols could be comparable to that of sub-micron aerosols. For example, on 8 November 2011 (day 152), the calculated aerosol heating effect increased by nearly 70 %, from $0.6\,\mathrm{K\,day^{-1}}$ to $1\,\mathrm{K\,day^{-1}}$, when we accounted for absorption due to super-micron particles. At the surface, aerosol forcing increased from $-6.8\,\mathrm{W\,m^{-2}}$ for $D_{1\,\mu\mathrm{m}}$ particles only to $-10.5\,\mathrm{W\,m^{-2}}$ for all aerosols.

4 Conclusions

We have analyzed the aerosol absorption and scattering coefficients for $D_{1\,\mu\mathrm{m}}$ and $D_{10\,\mu\mathrm{m}}$ particles for data collected over a period of 10 months during the GVAX campaign in Nainital, India. The primary conclusions drawn from this study are as follows:

1. Large particles ($D_{10\,\mu\mathrm{m}}$) exhibited markedly higher measured absorption values (by roughly 30 %) than smaller particles ($D_{1\,\mu\mathrm{m}}$) during several segments of the post-monsoon period.

2. The average absorption and scattering coefficients during the entire observation period were approximately $18\,\mathrm{M\,m^{-1}}$ and $206\,\mathrm{M\,m^{-1}}$, respectively. During the peak summer monsoon season (day < 100; roughly 50 % the entire observation period averages), the absorption and scattering coefficients were fairly low, with values of $7\,\mathrm{M\,m^{-1}}$ and $117\,\mathrm{M\,m^{-1}}$, respectively. These low values are attributable to washout of the aerosols. In this period, the absorption spectral index was also low (−0.7) compared to the average over the entire period (−0.95). The average scattering spectral index was also lower during the monsoon (−0.54) than during the entire period (−0.90), possibly because high levels of relative humidity (90 %) led to larger particles during the monsoon season.

ACPD
13, 19837–19852, 2013

3. Another striking feature found in the data was a marked increase in the absorption and scattering coefficients for the $D_{1\,\mu m}$ and $D_{10\,\mu m}$ particles in the last week of October through the second week of November. This increase was accompanied by a weaker wavelength dependence of absorption for $D_{10\,\mu m}$ particles, indicating an abundance of super-micron particles that absorb in all spectral ranges.

4. Back-trajectory analysis attributed the origin of super-micron aerosols to local pollution sources such as open trash burning and biofuel burning for cooking. Accounting for such aerosols increased the regional aerosol radiative forcing by roughly 50 %. The local source of the large absorbing aerosols is not known, but the population density in the valley surrounding Nainital suggests that these particles resulted from burning of trash. Because similar economic and habitation conditions are common in developing countries, large absorbing particles could be an important component of the regional-scale atmospheric energy balance.

Supplementary material related to this article is available online at: http://www.atmos-chem-phys-discuss.net/13/19837/2013/acpd-13-19837-2013-supplement.pdf.

Acknowledgements. This work was supported by the US Department of Energy, Office of Biological and Environmental Research, under contract DE-AC02-06CH11357.

References

Bahadur, R., Pravee, P. S., Xu, Y., and Ramanathan, V.: Solar absorption by elemental and brown carbon determined from spectral observations, P. Natl Acad. Sci. USA, 109, 17366–17371, doi:10.1073/pnas.1205910109, 2012.

Bergstrom, R. W., Russell, P. B., and Hignett, P.: Wavelength dependence of the absorption of black carbon particles: predictions and results from the TARFOX experiment and implications for the aerosol single scattering albedo. J. Atmos. Sci., 59, 568–578, 2002.

ACPD
13, 19837–19852, 2013

Bergstrom, R. W., Pilewskie, P., Russell, P. B., Redemann, J., Bond, T. C., Quinn, P. K., and Sierau, B.: Spectral absorption properties of atmospheric aerosols, Atmos. Chem. Phys., 7, 5937–5943, doi:10.5194/acp-7-5937-2007, 2007.

Chinnam, N., Dey, S., Tripathi, S. N., and Sharma, M.: Dust events in Kanpur, northern India: chemical evidence for source and implications to radiative forcing, Geophys. Res. Lett., 33, L08803, doi:10.1029/2005GL025278, 2006.

Costabile, F., Barnaba, F., Angelini, F., and Gobbi, G. P.: Identification of key aerosol populations through their size and composition resolved spectral scattering and absorption, Atmos. Chem. Phys., 13, 2455–2470, doi:10.5194/acp-13-2455-2013, 2013.

Dubovik, O., Holben, B., Eck, T. F., Mirnov, A. S., Kaufman, Y. J., King, M. D., Tanré, D., and Lutsker, I. S.: Variability of absorption and optical properties of key aerosols types observed in worldwide locations, J. Atmos. Sci., 59, 590–608, 2002.

Eck, T. F., Holben, B. N., Sinyuk, A., Pinker, R. T., Goloub, P., Chen, H., Chatenet, B., Li, Z., Singh, R. P., Tripathi, S. N., Reid, J. S., Giles, D. M., Dubovik, O., O'Neill, N. T., Smirnov, A., Wang, P., and Xia, X.: Climatological aspects of the optical properties of fine/coarse mode aerosol mixtures, J. Geophys. Res., 115, D19205, doi:10.1029/2010JD014002, 2010.

Gautam, R., Hsu, C. N., Kafatos, M., and Tsay, S. C.: Influences of winter haze on fog/low clouds over Indo-Gangetic plains, J. Geophys. Res.-Atmos., 112, D05207, doi:10.1029/2005JD007036, 2007.

Kim, D. Y. and Ramanathan, V.: Solar radiation budget and radiative forcing due to aerosols and clouds, J. Geophys. Res.-Atmos., 113, D02203, doi:10.1029/2007JD008434, 2008.

Kotamarthi, V. R.: Ganges Valley Aerosol Experiment Science and Operations Plan, available at: http://www.arm.gov/sites/amf/pgh/, 2011.

Lau, K. M. and Kim, K. M.: Observational relationships between aerosol and Asian monsoon rainfall, and circulation, Geophys. Res. Lett., 33, L21810, doi:10.1029/2006GL027546, 2006.

Ramanathan, V., Chung, C., Kim, D., Bettge, T., Buja, L., Kielh, J. T., Washington, W. M., Fu, Q., Sikka, D. R., and Wild, M.: Atmospheric brown clouds: impacts on South Asian climate and hydrological cycle, P. Natl. Acad. Sci. USA, 102, 5326–5333, doi:10.1073/pnas.0500656102, 2005.

Russell, P. B., Bergstrom, R. W., Shinozuka, Y., Clarke, A. D., DeCarlo, P. F., Jimenez, J. L., Livingston, J. M., Redemann, J., Dubovik, O., and Strawa, A.: Absorption Angstrom Exponent in AERONET and related data as an indicator of aerosol composition, Atmos. Chem. Phys., 10, 1155–1169, doi:10.5194/acp-10-1155-2010, 2010.

ACPD
13, 19837–19852, 2013

Sahai, S., Naja, M., Singh, N., Phanikumar, D. V., Dumka, U. C., Pant, V., Jefferson, A., Pant, P., Sagar, R., Satheesh, S. K., Krishna Moorthy, K., and Kotamarthi, V. R.: Evidence of perturbed aerosol physico-chemistry over Central Himalayas caused by post-harvest biomass burning in Punjab region during autumn season, Environ. Sci Technol., accepted, 2012.

ACPD
13, 19837–19852, 2013

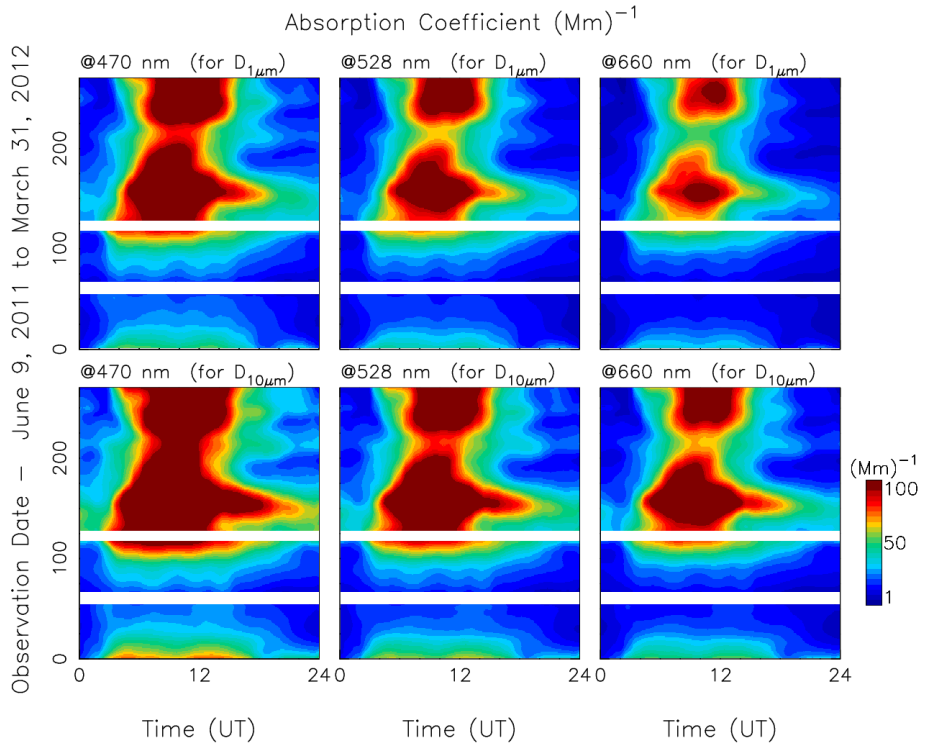

Fig. 1. Temporal and spectral variations of aerosol absorption. Daily variations of aerosol absorption coefficients in three wavelength bands – 470, 528 and 660 nm – for $D_{1\,\mu m}$ and $D_{10\,\mu m}$ particles from 9 June 2011 to 31 March 2012. Data are missing in the white areas.

ACPD
13, 19837–19852, 2013

Increased absorption by giant aerosol particles

V. S. Manoharan et al.

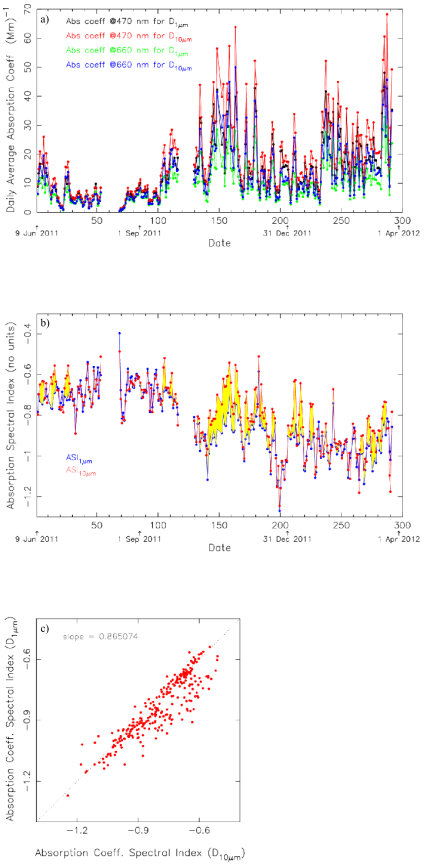

Fig. 2. Absorption properties of aerosols. **(a)** Time series of daily averaged absorption coefficient values at 470 and 660 nm for $D_{1\,\mu m}$ and $D_{10\,\mu m}$ particles. **(b)** Times series of daily averaged $ASI_{10\,\mu m}$ and $ASI_{1\,\mu m}$ values. The area shaded in yellow represents $ASI_{10\,\mu m} > ASI_{1\,\mu m}$. **(c)** Plot of $ASI_{10\,\mu m}$ vs. $ASI_{1\,\mu m}$, showing approximately 90 % correlation.

ACPD
13, 19837–19852, 2013

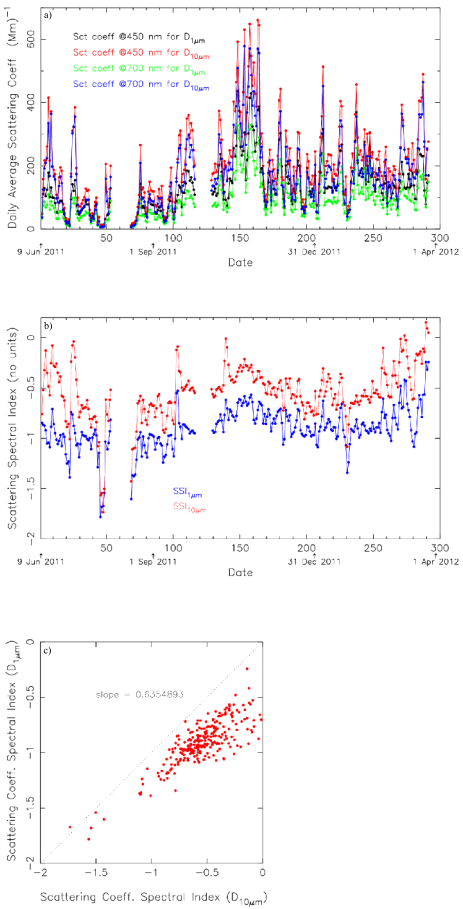

Fig. 3. Scattering properties of aerosols. **(a)** Time series of daily averaged scattering coefficient at 450 and 700 nm for $D_{1\,\mu m}$ and $D_{10\,\mu m}$ particles. **(b)** Times series of daily averaged values of $SSI_{10\,\mu m}$ and $SSI_{1\,\mu m}$. **(c)** Plot of $SSI_{10\,\mu m}$ vs. $SSI_{1\,\mu m}$, showing approximately 83 % correlation.

ACPD
13, 19837–19852, 2013

Increased absorption by giant aerosol particles

V. S. Manoharan et al.

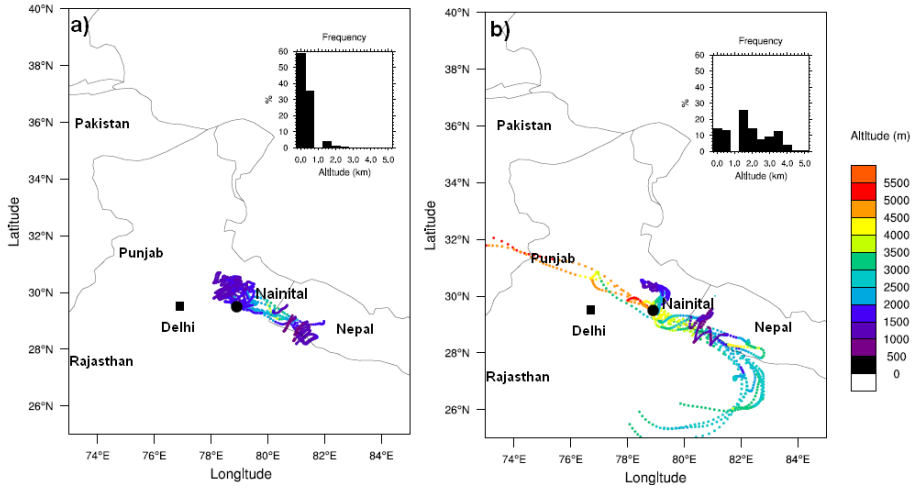

Fig. 4. Emission source analysis. Five-day HYSPLIT back-trajectories over Nainital, ending at **(a)** 0.5 km and **(b)** 2.5 km a.g.l.

ACPD
13, 19837–19852, 2013

Increased absorption by giant aerosol particles

V. S. Manoharan et al.